IET Renewable Power Generation

Special Issue: Oscillations in Power Systems with High Penetration of Renewable Power Generations

IET Journals
The Institution of Engineering and Technology

Electronic resistor emulators for ferroresonance damping in MV transformers

ISSN 1752-1416
Received on 28th February 2018
Revised 27th July 2018
Accepted on 14th September 2018
E-First on 5th November 2018
doi: 10.1049/iet-rpg.2018.5242
www.ietdl.org

Eduardo Bayona[1] ✉, Francisco Azcondo[1], Christian Brañas[1], Javier Diaz[1], Raquel Martínez[1], Mario Manana[1], Rafael Mínguez[2], Jose Ivan Rodríguez[2], Alberto Pigazo[1]

[1]*Depts. TEISA, IIE, IEE, University of Cantabria, Av/ Los Castros, 46, 39005. Santander, Spain*
[2]*Viesgo Electrical Distribution, c/ Isabel Torres, 25, 39011, Santander, Spain*
✉ *E-mail: eduardo.bayona@unican.es*

Abstract: The occurrence of ferroresonances, due to the presence of voltage transformers in isolated-neutral in medium-voltage (MV) distribution grids, results in overvoltages and overcurrents that may damage the connected equipment. To prevent this phenomenon, the protection windings of the MV transformers have to be properly loaded for damping purposes. Mitigation equipment based on resistors, passive/active circuits and static converters have been proposed in the literature. This study proposes a new variety of mitigation equipment based on very simple power electronic converters operated as configurable resistor emulators. The proposed approach is evaluated theoretically and validated experimentally. A resistor emulator proof of concept is designed and applied for damping ferroresonances due to the occurrence of line-to-ground faults in isolated-neutral MV distribution power systems.

Nomenclature

C_g	line-to-ground capacitance, F
C_o	resistor emulator capacitance, F
d	duty cycle
D	average duty cycle over $T = (2\pi/\omega)$
D_0	duty cycle at $v_\Delta = 0$
g_c	instantaneous resistor emulator conductance, S
G_c	conductance at $v_\Delta = 0$, S
H	magnitude of the linear controller
$\langle i_\Delta \rangle_{T_{sw}}$	open-delta current averaged over T_{sw}, A
$\langle i_L \rangle_{T_{sw}}$	inductor current averaged over T_{sw}, A
$\hat{i}_L$	peak current through L in each T_{sw}, A
k_d	slope of the duty cycle function, 1/V
k_G	slope of the conductance function, Ω
L	inductance of the converter, mH
ϕ_n	relative phase of v_Δ nth frequency component, V
R_d	damping resistance, Ω
R'_d	emulated damping resistance, Ω
R_L	resistor emulator load, Ω
r_s	current sensor resistance, Ω
t_{on}	on-time of the power device, μs
t_{off}	off-time of the power device, μs
T_d	damping time, s
T_{sw}	switching period of the power device, μs
v_Δ	protection windings voltage (open delta), V
$\hat{V}_{\Delta,n}$	amplitude of v_Δ nth frequency component, V
V_M	modulating signal peak value, V
V_o	converter output voltage, V
V_o	resistor emulator output voltage, V
ω	nominal grid frequency, rad/s

1 Introduction

The increasing penetration of distributed generation (DG) and storage systems in both low-voltage and medium-voltage (MV) electrical grids impacts on the electrical power quality [1]. Among other consequences, the presence of distributed resources under certain operation circumstances results in transitory abnormal oscillation states that the grid-connected DG and the electrical apparatus must cope with [2–4].

One of these irregular oscillation states is known as ferroresonance. It occurs when the non-linear characteristics of the passive elements, i.e. inductors saturation, are excited by certain events and an abnormal but stable oscillation state is reached [5, 6]. Inductive voltage transformers (IVTs) in MV isolated-neutral distribution grids, as shown in Fig. 1*a*, are prone to suffer ferroresonances after a circuit breaker operation, due to the parasitic line-to-ground capacitances [7]. These events cause voltage levels that occasionally exceeds the magnetisation knee of the VT, reaching a stable operation point different from the nominal one. Depending on the initial conditions, i.e. voltage phase, flux amplitude, equivalent line-to-ground capacitance and the VT magnetisation curve, one of the four potential ferroresonant modes is reached [8, 9]: fundamental, subharmonic, quasi-periodic or chaotic modes. As a result of the ferroresonance, overvoltages and overcurrents might damage the VT, electrovalves or other electrical apparatus.

To prevent the occurrence of ferroresonances, the employed VTs include two secondaries, the required measurement one and an optional protection winding, where the protection device is usually connected. Other approaches such as the connection of saturable inductances, at the MV level, are also possible but they are less common in isolated-neutral distribution power systems [10]. As illustrated in Fig. 1*a*, the protection windings of the three VTs are arranged to form an open delta, where the zero-sequence voltage is obtained. The most common protection strategy consists of connecting a damping resistor (R_d). If MV grid events result in VT saturation, a ferroresonance might occur depending on the line-to-ground parasitic capacitance (C_g), the operation conditions and the VT characteristics. R_d is designed to provide protection against the thermal damage caused by the MV grid transients, i.e. line-to-ground faults and, at the same time, damp the potential ferroresonance.

Commercial equipment for ferroresonance protection and proposals in the literature are based on [9, 11, 12]: non-electronic and electronic devices. The first ones use passive components such as resistors and saturable inductors to damp the abnormal oscillations. As a first approach, the whole frequency spectrum of

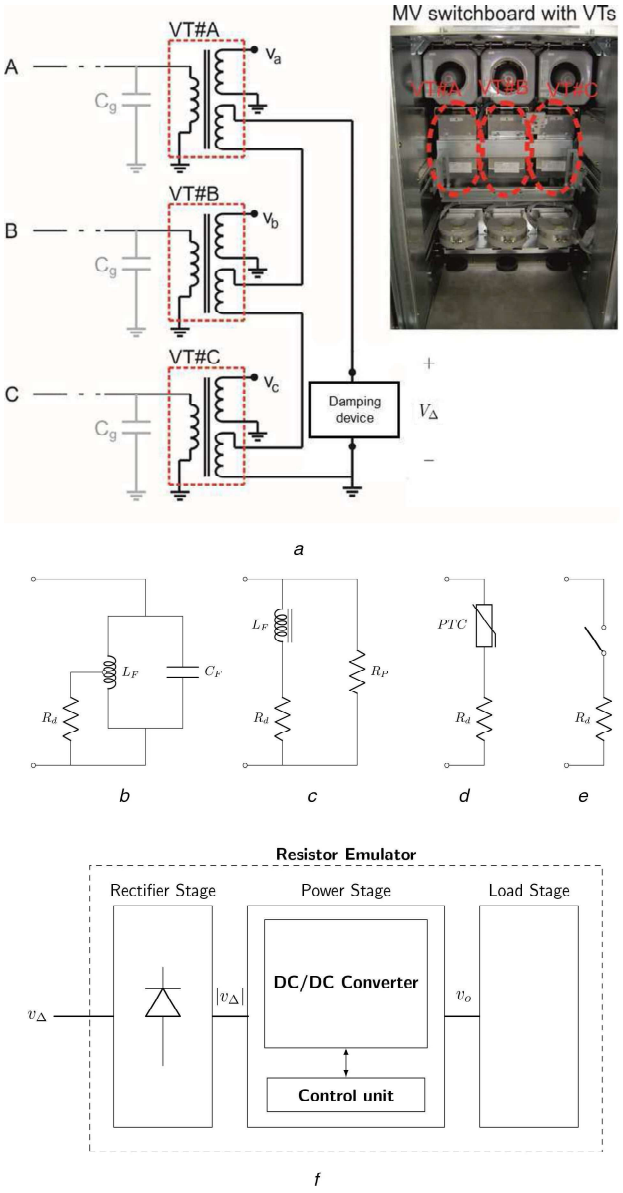

Fig. 1 *Voltage transformer (VT) configuration for voltage measurement in isolated-neutral MV distribution grids*

(a) General scheme with a damping device connected to open-delta protection windings, ***(b)*** Tuned passive filter, ***(c)*** Saturable reactance, ***(d)*** PTC resistor, ***(e)*** Electronic equipment based on static switches, ***(f)*** Proposed resistor emulator solution

the open-delta voltage (v_Δ) is compensated connecting a resistor that dissipates power, heating up the VT, during the event that stimulates the ferroresonance, i.e. certain line-to-ground faults. To alleviate this effect, in certain cases only some of the v_Δ harmonics, e.g. subharmonic ferroresonances, are damped by applying a tuned passive filter (Fig. 1*b*), avoiding power dissipation at the fundamental grid frequency (ω) [13]. An alternative approach consists of connecting a saturable reactance (Fig. 1*c*), which shows high impedance at ω and saturates faster than the VT in the occurrence of an overvoltage due to the ferroresonance [14]. Alternatively, a positive thermal coefficient (PTC) resistor is employed in [15] (Fig. 1*d*). Thermal damage in the VT is prevented as the PTC resistance increases from a very small value to several hundred ohms or more in few seconds as the current goes through it [9]. It must be considered that to avoid an unwanted operation of the PTC, due to natural network asymmetries or disturbances, a threshold voltage is commonly defined and the PTC is disconnected below this voltage level.

Electronic-based equipment consists of solid-state devices employed as static switches, and a damping resistor that connects and disconnects to the VT protection secondary [16] (Fig. 1*e*). This equipment shows a faster response than the non-electronic solutions, avoiding the VT loading during the fault and providing a relatively smooth ferroresonance damping. However, their main drawbacks are that the bulky R_d is still required [17, 18], their performance is limited by the employed on/off controller [19] and the switching frequency is low [20].

Alternatively to the strategies found in the literature, this paper explores the applicability of well known power converter stages, i.e. [21–25], loss-free resistor (LFR) emulators for the mitigation of ferroresonances in MV VTs (Fig. 1*f*). The concept of the resistive emulator has been recently introduced in the literature in order to compensate oscillations in both DC [26] and AC [27] grids. These converters achieve a fast and an adjustable response, maximising the power density. This paper generalises the approach given in [27] and provides a design methodology applicable to resistive emulators in AC grids. By eliminating the output voltage control, included in power factor correction (PFC) applications, it is imposed that the emulated damping resistance (R'_d) is dependent on v_Δ. Applicable resistor emulator topologies, with emphasis on non-linear current control, and inherent LFR response, are presented in Section 2 and their response under a ferroresonance occurrence is modelled. The most promising approach is evaluated experimentally in Section 3. Finally, the conclusions of this work are provided in Section 4.

2 Resistor emulators for ferroresonance mitigation

The instantaneous open-delta voltage including the fundamental component, subharmonic and quasi-periodic ferroresonances is described by

$$v_\Delta(t) = \sum_{n=0}^{\infty} \hat{V}_{\Delta,n} \sin(n\omega t + \phi_n) \tag{1}$$

where ω is the fundamental grid frequency, $n \in \mathbb{R}^+$ allows the consideration of both integer and non-integer multiples of ω and $\hat{V}_{\Delta,n}$ and ϕ_n are the amplitude and relative phase of the $v_\Delta n$th frequency component.

The performance of the resistor emulators depends on the ferroresonance mode and the equivalent resistance connected to the open delta during the ferroresonance. The analysed resistor emulators for ferroresonance damping are depicted in Fig. 2, where only the DC/DC converter is shown.

2.1 Boost resistor emulator

The boost converter in Fig. 2*a* can be controlled following diverse approaches to work as LFR [21]. For example, assuming ideal switching transients with no reverse current, establishing a constant conduction time (t_{on}) and ensuring operation in the boundary between discontinuous conduction mode (DCM) and the continuous CM (CCM), i.e. critical CM (CrCM), without any further current controller, the averaged emulated resistance over each switching period (T_{sw}) is

$$R'_d = \frac{2L}{t_{on}} \tag{2}$$

where L is the DC/DC converter inductance.

The parameter t_{on} modulates R'_d. The simplest approach consists on maintaining t_{on} constant, which results in a constant R'_d, defined by (2), in both the unperturbed situation and under a ferroresonance event. By adjusting t_{on}, as a function of v_Δ, a more complex behaviour can be emulated, e.g. $t_{on} = 0$ ($R'_d \to \infty$) for no mitigation operation and $t_{on} > 0$, constant or depending on v_Δ, during the ferroresonance. The last approach requires including identification and decision stages in the controller.

Also implementing a peak current non-linear control (PCNLC) [28], the input current is controlled, and the equivalent resistance emulated by the converter is

$$R'_{\mathrm{d}} \simeq r_{\mathrm{s}} \frac{V_{\mathrm{o}}}{V_M} \tag{3}$$

with r_{s}, V_{o} and V_{M} being the current sensor resistance, output voltage and carrier signal peak value, respectively.

To increase the accuracy of the emulated resistance, the PCNLC can be modified by including a dual ramp [29] and, then, the average input current becomes proportional to the input voltage

$$V_M \frac{v_\Delta}{V_0} = r_{\mathrm{s}} \langle i_{\mathrm{L}} \rangle_{T_{\mathrm{sw}}} = r_{\mathrm{s}} \langle i_\Delta \rangle_{T_{\mathrm{sw}}} \tag{4}$$

where $\langle i_{\mathrm{L}} \rangle_{T_{\mathrm{sw}}}$ and $\langle i_\Delta \rangle_{T_{\mathrm{sw}}}$ are the inductor current and the open-delta current averaged over T_{sw}, resulting in an equivalent resistance

$$R'_{\mathrm{d}} = r_{\mathrm{s}} \frac{V_{\mathrm{o}}}{V_M} \tag{5}$$

Input current sensing is required with this approach and the values of R'_{d} can be adjusted by modifying the ratio V_{O}/V_M. The required R'_{d} values for damping purposes must be considered during the design stage in order to select the converter components, which limits the adaptability of this approach to certain practical ferroresonance conditions.

To keep the controller as simple as possible, while achieving the fastest response, an attractive option for the boost resistor emulator is selecting the CrCM as operation mode [21]. Then, the above-presented t_{on} time control or a simple switching controller, i.e. L6560 integrated circuit (IC) or its upgrades, can be applied. From Fig. 2*a*

$$\begin{cases} L \dfrac{\hat{i}_{\mathrm{L}}}{t_{\mathrm{on}}} = v_\Delta \\ L \dfrac{\hat{i}_{\mathrm{L}}}{t_{\mathrm{off}}} = v_\Delta - V_{\mathrm{o}} \end{cases}, \tag{6}$$

where $\hat{i}_{\mathrm{L}}$ and t_{off} are the peak current through L and the off-time of the switching power device. To achieve a resistor emulation, the following relationship must be fulfilled:

$$2\langle i_{\mathrm{in}} \rangle_{T_{\mathrm{sw}}} = g_{\mathrm{c}} v_\Delta = \hat{i}_{\mathrm{L}} \tag{7}$$

By replacing $t_{\mathrm{on}} = \mathrm{d}T_{\mathrm{sw}}$ and $t_{\mathrm{off}} = (1-d)T_{\mathrm{sw}}$ in (6), being d the instantaneous duty cycle, the CrCM requires

$$T_{\mathrm{sw}} = L\, g_{\mathrm{c}} \left(1 + \frac{v_\Delta}{v_\Delta - V_{\mathrm{o}}}\right) \tag{8}$$

where g_{c}, the instantaneous resistor emulator conductance, is the selected control parameter. Hence, within each switching period

$$R'_{\mathrm{d}} = \frac{v_\Delta}{\langle i_{\mathrm{in}} \rangle_{T_{\mathrm{sw}}}} = \frac{2}{g_{\mathrm{c}}} \tag{9}$$

The control parameter in the simplest approach, g_{c}, is kept constant, which results in a constant emulated resistance matching (9). More advanced behaviours are achieved by varying g_{c} as a function of v_Δ, identically to the implementation in which t_{on} is the control parameter.

Linear- or hysteresis-based non-linear controllers can also be applied to the boost PFC to achieve an equivalent resistive behaviour

$$\langle i_\Delta \rangle_{T_{\mathrm{sw}}} r_{\mathrm{s}} = H\, v_\Delta \tag{10}$$

where H depends on the selected linear controller, hence, the equivalent input resistance is defined by

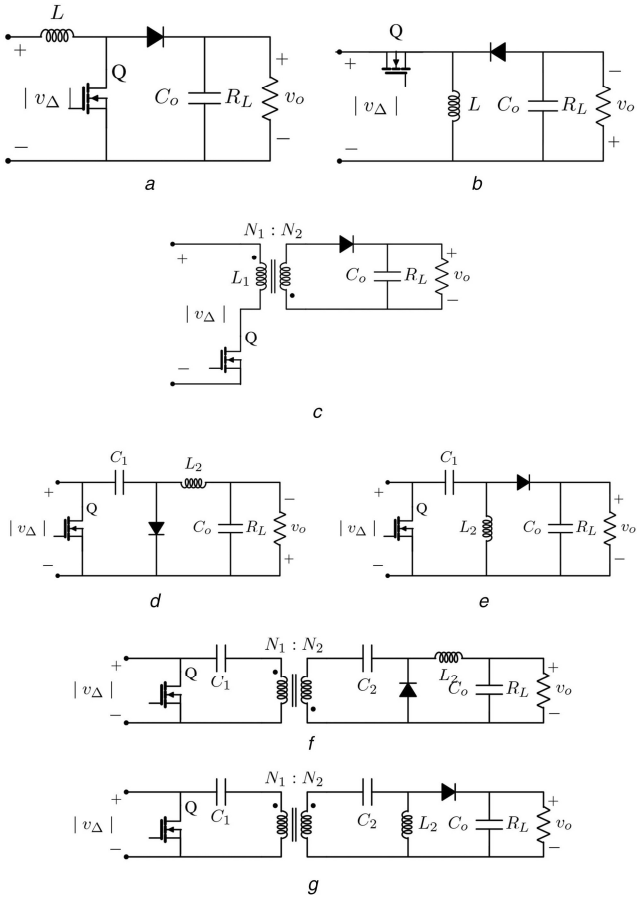

Fig. 2 *Evaluated topologies for resistor emulation, full diode bridge plus*
(a) Boost converter, ***(b)*** Buck–boost converter, ***(c)*** Flyback converter, ***(d)*** Ćuk converter, ***(e)*** SEPIC converter, ***(f)*** Isolated Ćuk converter, ***(g)*** Isolated SEPIC converter
Note: $L1$ (not shown) in Ćuk and SEPIC converters are connected between the AC line and the diode bridge

$$R'_{\mathrm{d}} = \frac{r_{\mathrm{s}}}{H}. \tag{11}$$

It must be considered that, depending on the ferroresonance spectral characteristics, H changes according to the designed linear controller. As a consequence, the controller must not only take into account conventional issues in these converters, i.e. stability and overshoot but also the fastest response to cover the spectral content of the ferroresonance to be damped.

In this application, there are no specific DC load requirements to be fulfilled. A controller with a simple activation leads to a constant R'_{d}. The analysis provided with each control mode shows that more advanced behaviour can be achieved by adjusting the control parameter as a function of v_Δ. However, it must be considered that sudden v_Δ increasing may not be damped fast enough due to the limitations of the boost topology, i.e. $V_{\mathrm{o}} > \hat{V}_{\Delta,n}$, and the dynamic response dependence on the output capacitance and load.

2.2 Buck–boost resistor emulator

The buck–boost resistor emulator in Fig. 2*b* [22] avoids the voltage limitation $V_{\mathrm{o}} > \hat{V}_{\Delta,n}$ imposed by the boost converter. Following the analysis in the previous section, the converter operated in DCM with constant switching period (T_{sw}) and duty cycle (D) has the LFR property and shows the equivalent input resistance in each T_{sw}:

$$R'_{\mathrm{d}} = \frac{2L}{D^2 T_{\mathrm{sw}}} \tag{12}$$

where L corresponds to the inductance of the converter inductor in Fig. 2*b*. Since T_{sw} and D are kept constant during the ferroresonance, R'_d matches (12). As in the boost case, a stronger ferroresonance mitigation action is achieved by adjusting D as a function of v_Δ. By assuming $d = D_0 + k_d v_\Delta$, the obtained emulated resistance becomes

$$R'_d = \frac{2L}{D_0^2 T_{sw}} \frac{1}{1 + v_\Delta k_d \left((4/D_0) + (v_\Delta k_d / D_0^2)\right)} \tag{13}$$

where R'_d decreases with $|v_\Delta|$ if the parameter k_d is kept constant. However, k_d can be varied to achieve the required R'_d.

The operation of the buck–boost converter in the CrCM results in a close to an LFR behaviour, reducing $\hat{i}_L$ with respect the DCM, while providing adjustment ability of R'_d [22].

As the first approach, a t_{on} is selected as a control parameter. By keeping $t_{on} = T_{on}$ constant

$$R'_d = \frac{2L}{T_{ON}} \left(1 + \frac{v_\Delta}{V_o}\right) \tag{14}$$

The minimal value R'_d is adjusted by means of $2L/T_{ON}$ and the maximum value depends on the allowable v_Δ/V_o ratio. By properly selecting the output capacitance and resistance, i.e. slowing down the charging transient, the R'_d is kept large until the ferroresonance occurs, when the output voltage is large enough to reduce R'_d and damp the ferroresonance. The selection of the most suitable values requires a previous analysis of the ferroresonance events.

Similarly, and following the analysis in [23] using the L6560 ICs for operation in CrCM, the emulated resistance within each switching period is obtained as:

$$R'_d = \frac{2(1 + (v_\Delta/V_o))}{g_c} \tag{15}$$

where $g_c = (\hat{i}_\Delta / v_\Delta)$ is set constant and, then, $g_c \simeq G_c = (I_\Delta / V_\Delta)$, where I_Δ and V_Δ are the effective values of the resistor emulator input current and open-delta voltage, respectively. The control parameter here is g_c and, similarly to the case with T_{ON} as control parameter, the output capacitance and resistance are selected to adjust the ratio v_Δ/V_o.

Assuming a periodic ferroresonance mode, the equivalent input resistance is obtained by averaging (15) over a ferroresonance semi-period

$$\langle R'_d \rangle_{T_{FR}/2} = \frac{2}{T_{FR}} \int_0^{T_{FR}/2} \langle R'_d \rangle_{T_{sw}}(\tau)\, d\tau \tag{16}$$

where $(T_{FR}/2) = \max(\pi/n\omega)$.

By evaluating (16), the equivalent input resistance during the ferroresonance is obtained (see (17)) where $m = \min(n)$. From (17), the equivalent input resistance depends on the ferroresonance mode and the output voltage V_o and an adaptive R'_d is obtained during the ferroresonance occurrence.

Under the assumption of fundamental and subharmonic ferroresonances, where all the spectral components of v_Δ are integer multiples of m [8], i.e. $i = (n/m) \in \mathbb{Z}^+$, (17) is rewritten as

$$\langle R'_d \rangle_{T_{FR}/2} = \frac{2}{g_c} \left(1 + \frac{2\hat{V}_{\Delta,m} + \sum_{i=3,5,\ldots} (\hat{V}_{\Delta,im}/i) \cos\phi_{im}}{\pi V_o}\right) \tag{18}$$

$$\langle R'_d \rangle_{T_{FR}/2} = \frac{2}{g_c} \left(1 + \frac{\sum_{n=0}^{\infty} (\hat{V}_{\Delta,n}/(n/m))(\cos\phi_n - \cos(\phi_n + \pi(n/m)))}{\pi V_o}\right) \tag{17}$$

Table 1 Emulated damping resistance due to the resistor emulators

	DCM	CrCM
boost	$\frac{2L}{D_0^2 T_{sw}}\left(\frac{1}{1-(v_\Delta/v_o)}\right)$	$\frac{2L}{T_{ON}}$
buck–boost	$\frac{2L}{D_0^2 T_{sw}}$	$\frac{2L}{T_{ON}}\left(1+\frac{v_\Delta}{v_o}\right)$
flyback	$\frac{2L_1}{D_0^2 T_{sw}}$	$\frac{2L_1}{T_{ON}}\left(1+\frac{N_2}{N_1}\frac{v_\Delta}{v_o}\right)$
Ćuk	$\frac{2L_{eq}}{D_0^2 T_{sw}}$	$\frac{2L_{eq}}{T_{ON}}\left(1+\frac{v_\Delta}{v_o}\right)$
isolated Ćuk	$\frac{2L_{eq}}{D_0^2 T_{sw}}$	$\frac{2L_{eq}}{T_{ON}}\left(1+\frac{N_2}{N_1}\frac{v_\Delta}{v_o}\right)$
SEPIC	$\frac{2L_{eq}}{D_0^2 T_{sw}}$	$\frac{2L_{eq}}{T_{ON}}\left(1+\frac{v_\Delta}{v_o}\right)$
isolated SEPIC	$\frac{2L_{eq}}{D_0^2 T_{sw}}$	$\frac{2L_{eq}}{T_{ON}}\left(1+\frac{N_2}{N_1}\frac{v_\Delta}{v_o}\right)$

With non-isolated: $L_{eq} = (L_1 L_2/(L_1 + L_2))$, isolated: $L_{eq} = \left(L_1 L_2 / \left(L_1 (N_2/N_1)^2 + L_2\right)\right)$.

From [8], $\hat{V}_{\Delta,im}$ decreases by increasing i and vice versa for fundamental and subharmonic ferroresonances, respectively.

In the case of a pure sinusoidal ferroresonance, $m = n$ and $\phi_n = 0$, (18) is simplified to

$$R'_d = \frac{2}{g_c}\left(1 + \frac{2\hat{V}_\Delta}{\pi V_o}\right) \tag{19}$$

The parameter g_c in (15) is kept constant but, alternatively, it can be adjusted, $g_c = G_c + k_G v_\Delta$ and, then, (15) becomes

$$R'_d = \frac{2}{G_c + k_G v_\Delta}\left(1 + \frac{v_\Delta}{V_o}\right) \tag{20}$$

which results in the emulated resistance

$$R'_d = \frac{2}{G_c} \cdot \frac{1}{1 + (2v_\Delta k_G/G_c) + (v_\Delta^2 k_G / G_c V_0)} \tag{21}$$

This provides an extra modulation capability of the mitigation action by decreasing R'_d with k_G.

2.3 Other applicable topologies

Following the analysis given in the previous sections, other power converter topologies without output voltage regulation can be applied for ferroresonance damping. These topologies include Ćuk and single ended primary inductor converter (SEPIC) and its isolated versions, as the most representative fourth-order converters, as depicted in Fig. 2. The emulated damping resistances corresponding to these topologies are summarised in Table 1, where DCM and CrCM approaches are evaluated.

The topologies presented in Fig. 2 obtain an LFR behaviour with no input to output voltage relation restrictions and results in the same R'_d expression. While the buck–boost (flyback) is the simplest configuration, Ćuk and SEPIC topologies lower the input current peaks, noise and, therefore, input filter requirements because input current circulates during t_{on} and t_{off}.

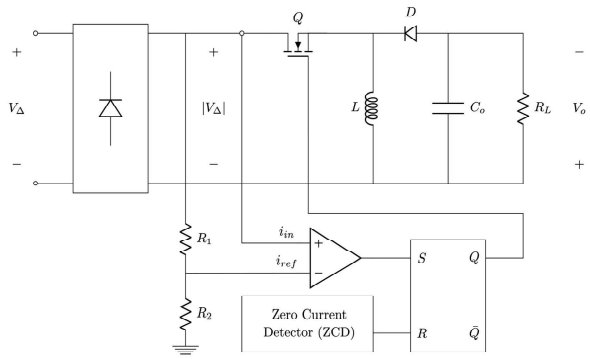

Fig. 3 *Buck–boost resistor emulator with the CrCM controller*

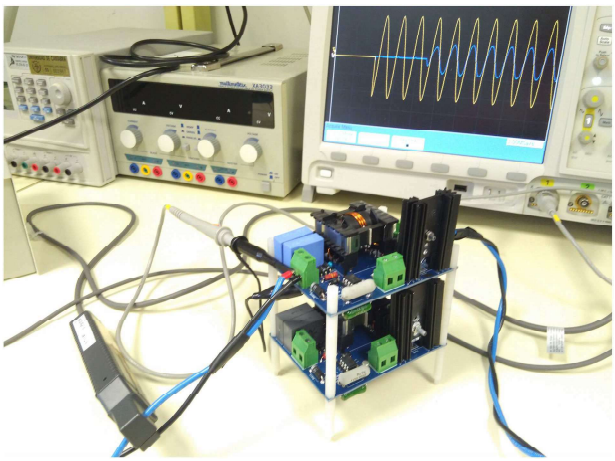

Fig. 4 *Developed buck–boost resistor emulator*

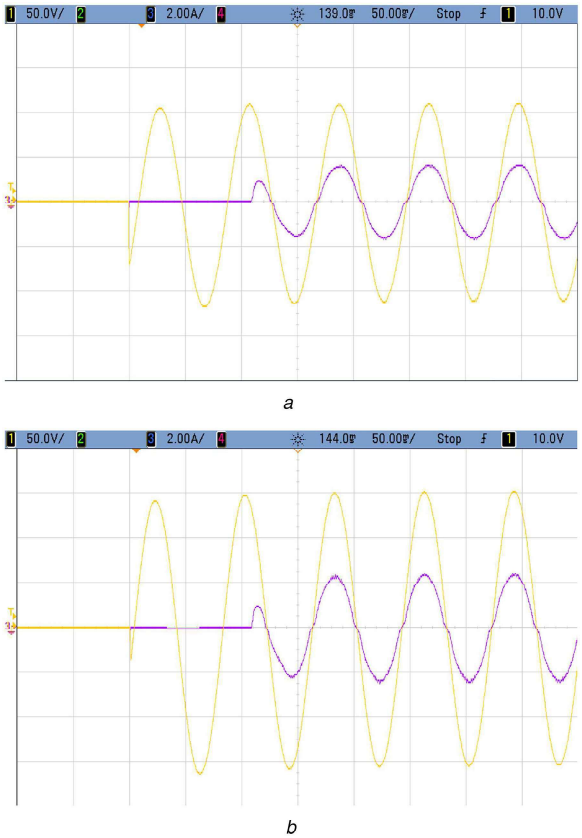

Fig. 5 *Experimental characterisation of the buck–boost resistor emulator at nominal resistance R_L and ferroresonance with $n = 0.25$ (12.5 Hz)*
(a) $V_\Delta = 80\,\mathrm{V^{rms}}$, ***(b)*** $V_\Delta = 110\,\mathrm{V^{rms}}$

3 Example of resistor emulator design based on the buck–boost converter operated in CrCM

The different solutions analysed in Section 2 are capable of adjusting the emulated R'_d as a function of a modulator parameter, e.g. t_on for the operation in DCM, i_peak for the operation in the CrCM, V_m for the NLC and the reference current for the linear control with k as an extra parameter to reinforce the mitigation action if required. The Appendix describes an applicable procedure to select the resistive emulator components depending on the MV grid and ferroresonance characteristics. Below, the specific implementation based on the buck–boost topology and the IC L6560 is described.

The buck–boost resistor emulator in CrCM has been selected due to the inherent dependency of R'_d on v_Δ and, the L6560 is selected as controller IC (Fig. 3). Prior to the rectification stage, an EMI filter is included for removing high-frequency harmonics generated by the high-frequency switched resistor emulator. The AC mains voltage is rectified by a diode bridge and the rectified voltage supplies the buck–boost converter. The converter is completed with the load resistor R_L and a low-ESR output capacitor with enough energy storage capacity to guarantee a good transient performance. Although the L6560 is designed to control PFC, in this application, the output voltage control is removed for a proper operation as an LFR emulator. Instead, a constant value for the error signal is used to feed the current loop multiplier and so multiplied by a measurement of the rectified input voltage, as shown in Fig. 3. This reference current is fed into the current comparator with the inductor current signal. As the instantaneous inductor current equals the reference current in the comparator, the conduction of the metal–oxide–semiconductor field-effect transistor (MOSFET) is terminated. After the MOSFET turn-off, the buck–boost inductor discharges its energy into the load until its instant current reaches zero activating the zero current detectors (ZCDs) and driving the MOSFET on again, starting another conversion cycle. The ZCD of the controller is connected to an auxiliary winding of the inductor through a limiting resistor. The ZCD circuit is negative-going edge-triggered, so that when the voltage on the pin falls below a threshold value, the pulse-width modulation latch is set and the MOSFET is turned on. The ZCD circuit will be rearmed when the voltage exceeds a certain value due to MOSFET's turn-off. The g_c value of the resistor emulator is established according to the safe operation area of the selected MOSFET, so that the R'_d range is limited within the safe operation parameters of the emulator.

4 Experimental results

To achieve repetitive tests and carry out a fair evaluation, a programmable AC source is employed to emulate subharmonic ferroresonances at different voltages and frequencies. The developed resistor emulator prototype, based on the buck–boost topology is shown in Fig. 4. The captured voltage and current waveforms are post-processed to evaluate the experimental equivalent resistance.

The resistor emulator has been evaluated with pure sinusoidal voltage signals emulating the characteristic frequencies found in subharmonic ferroresonances.

In isolated-neutral power systems, the amplitude of v_Δ during the fault is limited by the line-to-line voltage. In this case, $\hat{V}_{\Delta,\,0.25} = 150\,\mathrm{V}$ is the maximum voltage measured during faults. The distribution system operator (DSO) specifies the target R'_d provided by the resistor emulator during the ferroresonance for an appropriate mitigation, in correspondence to the employed VTs and the equivalent line-to-ground capacitance. The target R'_d is $60\,\Omega$. Moreover, the system protections are configured to limit the overvoltage duration, and the resistor emulator operation time to 6 s. G_c, L, C and R_L are selected according to these specifications.

Figs. 5*a* and *b* show the obtained results at 12.5 Hz. Afterwards, the resistor emulator activates, the input current reaches the steady state in less than half cycle. Similar behaviour is observed at 25 Hz, as it is shown in Figs. 6*a* and *b*. The measured R'_d within these

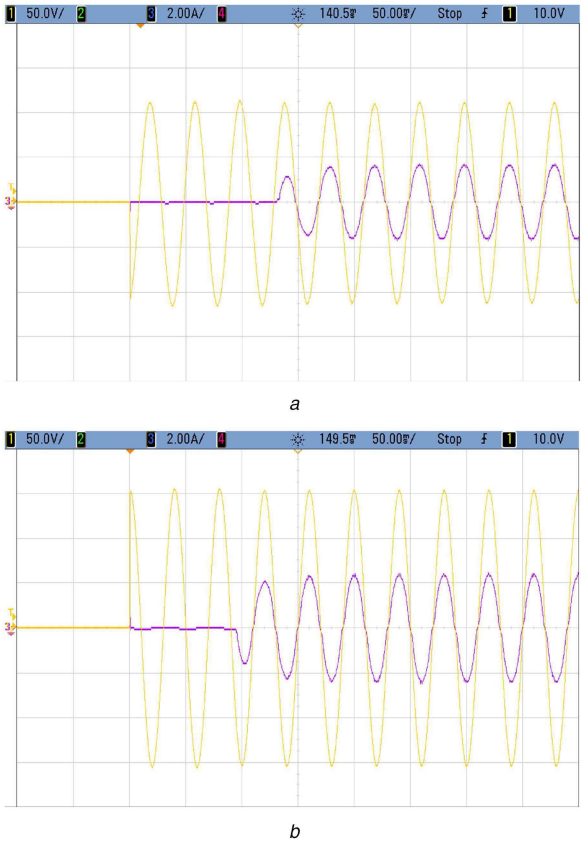

Fig. 6 *Experimental characterisation of the buck–boost resistor emulator at nominal resistance R_L and ferroresonance with $n = 0.5$ (25 Hz)*

(a) $V_\Delta = 80\ \mathrm{V^{rms}}$, ***(b)*** $V_\Delta = 110\ \mathrm{V^{rms}}$

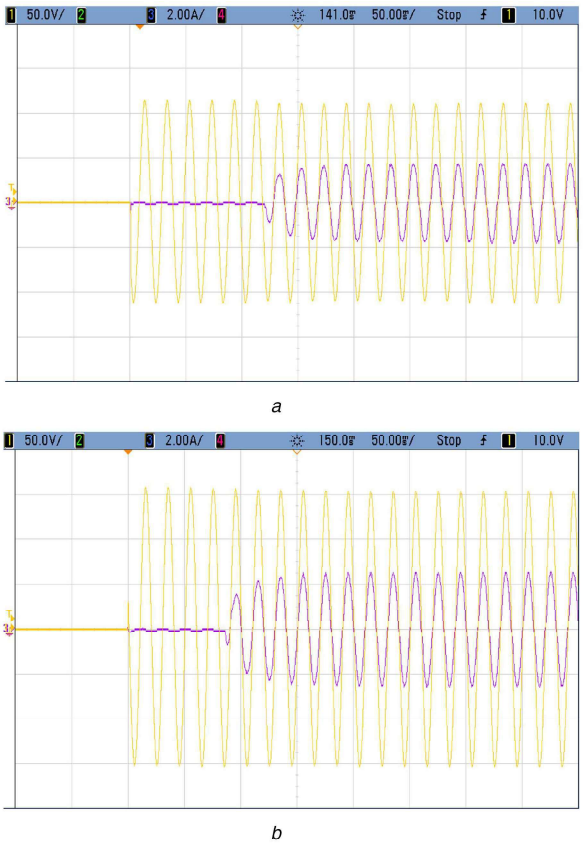

Fig. 7 *Experimental characterisation of the buck–boost resistor emulator at 50 Hz ($n = 1$) and double $R_L = 2R_{L,nominal}$*

(a) $V_\Delta = 80\ \mathrm{V^{rms}}$, ***(d)*** $V_\Delta = 110\ \mathrm{V^{rms}}$

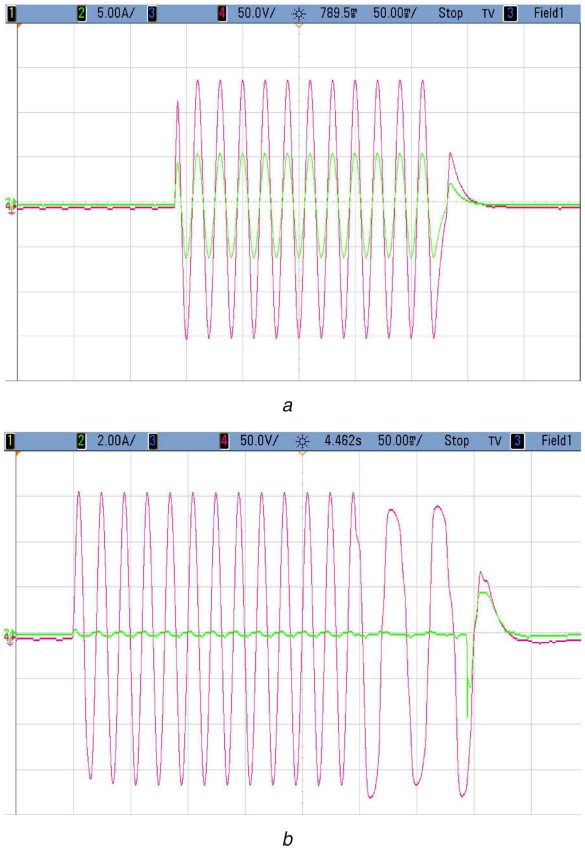

Fig. 8 *Ferroresonance mitigation*

(a) Damping resistor (25 Ω): in continuous operation during the fault and the ferroresonances (50 V/div, 5 A/div and 50 ms/div), ***(b)*** Resistor emulator: activated at 110 ms since the ferroresonance occurrences (50 V/div, 2 A/div and 50 ms/div)

voltage values is in the [63, 68 Ω] range. The value of G_c has been selected according to the equivalent resistance range and, hence, the applied power variation within the considered peak values of the open-delta voltage [40–150 V_{rms}]. The equivalent resistance is kept invariant to the tested frequency changes and only the amplitude of the open-delta voltage changes the measured R'_d.

The effect of doubling the resistor emulator DC load (R_L) at 50 Hz is shown in Fig. 7. By doubling the applied R_L, the observed transient response is smoother and longer but, again, the obtained equivalent resistance can be adjusted by means of G_c and, with the doubled R_L, the measured R'_d range widens to [61, 70 Ω].

To validate the analysis in Section 2 and the previous results, the effect of a damping resistor ($R_d = 25\,\Omega$) and the developed resistor emulator have been tested under real subharmonic ferroresonance conditions. The occurrence of faults results in overvoltages at the open-delta protection windings and saturation of the VTs and, as consequence, a ferroresonance is excited. The voltage and current waveforms measured in the case of the damping resistor are shown in Fig. 8*a*. In normal conditions, the open-delta voltage is zero and, due to the fault, the open-delta voltage increases. The power consumption could damage the VT if its nominal power is exceeded. Once the ferroresonance occurs, R_d mitigates the ferroresonance in <30 ms. The damping resistor was replaced by the resistor emulator and the obtained results are shown in Fig. 8*b*. The resistor emulator maintains a negligible power consumption during the fault. After the ferroresonance occurrence and in the steady state, the controller activates the resistor emulator mitigating the ferroresonance in <50 ms.

The ferroresonance event is longer in the case of the resistor emulator but this time is programmed to keep it limited to 100 ms, within the applicable tripping time of fault protection equipment, typically in the range of seconds. The dissipated energy in the VT terminals in the case of the resistor emulator matches the required

energy to mitigate the phenomenon and it does not load the VTs during the fault.

5 Conclusion

A new application of well known power converters acting as LFR emulators to damp ferroresonances in VTs has been presented. Buck–boost-type converters including fourth- order topologies operating in the DCM, CrCM or in CCM with NLC have been proposed as active ferroresonance mitigators in VT. The configurable emulated resistance defines an adequate trade-off between ferroresonance extinction and VT protection by defining the damping time and the power dissipated in the VT, taking into account the severity of the ferroresonance and the applicable standard. Considering the control simplicity and the fast dynamic response, the buck–boost converter operating in the CrCM is selected to test the performance in laboratory conditions and under real ferroresonance occurrence. The given experimental results obtained in a laboratory setup prove the effective mitigation of ferroresonances.

6 Acknowledgments

This work was supported by the Spanish government and FEDER funds of the European Union under RETOS RTC-2015-4176-3, *Innovation in the automation of the isolated neutral distribution.* The authors also acknowledge the support received from Viesgo S.L.

7 References

[1] Bollen, M.H., Hassan, F.: '*Integration of distributed generation in the power system*' (Wiley-IEEE Press, Hoboken, NJ, USA, 2011), ISBN 9780470643372

[2] Mozina, C.J.: 'Impact of smart grids and green power generation on distribution systems', *IEEE Trans. Ind. Appl.*, 2013, **49**, (3), pp. 1079–1090, doi: 10.1109/tia.2013.2253292

[3] Esmaeili, M., Rostami, M., Gharehpetian, G.B., *et al.*: 'Ferroresonance after islanding of synchronous machine-based distributed generation', *Can. J. Electr. Comput. Eng.*, 2015, **38**, (2), pp. 154–161, doi: 10.1109/cjece.2015.2411713

[4] Rezaei-Zare, A., Etemadi, A.H., Iravani, R.: 'Challenges of power converter operation and control under ferroresonance conditions', *IEEE Trans. Power Deliv.*, 2017, **32**, (6), pp. 2380–2388, ISSN 0885-8977, doi: 10.1109/TPWRD.2016.2626266

[5] Fuchs, E., Masoum, M.A.S.: '*Power quality in power systems and electrical machines*' (Academic Press, London, UK, 2015, 2nd edn.), ISBN 9780128007822

[6] Yang, M., Sima, W., Yang, Q., *et al.*: 'Non-linear characteristic quantity extraction of ferroresonance overvoltage time series', *IET Gener. Transm. Distrib.*, 2017, **11**, (6), pp. 1427–1433, doi: 10.1049/iet-gtd.2016.0873

[7] Mellik, T.A., Dionise, T.J., Yanniello, R.: 'A case study of voltage transformer failures: solution implementation in a modern data', *IEEE Ind. Appl. Mag.*, 2018, **24**, (1), pp. 98–109, doi: 10.1109/mias.2016.2600682

[8] Ferracci, P.: 'Ferroresonance'. Cahier Technique 190, Group Schneider, 1998

[9] Price, E.: 'A tutorial on ferroresonance'. Proc. 67th Annual Conf. Protective Relay Engineers, College Station, TX, USA, March 2014, pp. 676–704, doi: 10.1109/CPRE.2014.6799036

[10] Radmanesh, H., Heidary, A., Gharehpetian, G.B., *et al.*: 'Dual function ferroresonance and fault current limiter based on DC reactor', *IET Gener. Transm. Distrib.*, 2016, **10**, (9), pp. 2058–2065, doi: 10.1049/iet-gtd.2015.1032

[11] Venkatesh, C., Shanti Swarup, K.: 'Performance assessment of distance protection fed by capacitor voltage transformer with electronic ferro-resonance suppression circuit', *Electr. Power Syst. Res.*, 2014, **112**, pp. 12–19, doi: 10.1016/j.epsr.2014.03.003

[12] Khan, S.A., Bakar, A.H.A., Rahim, N.A., *et al.*: 'Analysis of ferroresonance suppression and transient response performances for various ferroresonance suppression circuits in capacitive voltage transformers'. Proc. Third IET Int. Conf. Clean Energy and Technology (CEAT) 2014, Kuching, Malaysia, November 2014, pp. 1–6, doi: 10.1049/cp.2014.1474

[13] Shahabi, S., Mirzaei, M., Gholami, A., *et al.*: 'Investigation of performance of ferroresonance suppressing circuits in coupling capacitor voltage transformers'. Proc. Fourth IEEE Conf. Industrial Electronics and Applications, Xi'an, China, May 2009, pp. 216–221, doi: 10.1109/ICIEA.2009.5138199

[14] Olguín-Becerril, M.A., Angeles-Camacho, C., Fuerte-Esquivel, C.R.: 'Ferroresonance in subharmonic 3rd mode in an inductive voltage transformer, a real case analysis', *Int. J. Electr. Power Energy Syst.*, 2014, **61**, pp. 318–325, doi: 10.1016/j.ijepes.2014.03.057

[15] Piasecki, W., Florkowski, M., Fulczyk, M., *et al.*: 'Mitigating ferroresonance in voltage transformers in ungrounded MV networks', *IEEE Trans. Power Deliv.*, 2007, **22**, (4), pp. 2362–2369, doi: 10.1109/tpwrd.2007.905383

[16] Sima, W., Yang, M., Yang, Q., *et al.*: 'Simulation and experiment on a flexible control method for ferroresonance', *IET Gener. Transm. Distrib.*, 2014, **8**, (10), pp. 1744–1753, doi: 10.1049/ietgtd.2014.0046

[17] Li, Y., Shi, W., Qin, R., *et al.*: 'A systematical method for suppressing ferroresonance at neutral-grounded substations', *IEEE Trans. Power Deliv.*, 2003, **18**, (3), pp. 1009–1014, doi: 10.1109/tpwrd.2003.813858

[18] Ryzhkova, Y.N., Tsyruk, S.A.: 'Ferroresonance suppression in distribution networks'. Proc. Applications and Manufacturing (ICIEAM) 2016 Second Int. Conf. Industrial Engineering, Chelyabinsk, Russia, May 2016, pp. 1–4, doi: 10.1109/ICIEAM.2016.7911458

[19] Navaei, M., Abdoos, A.A., Shahabi, M.: 'A new control unit for electronic ferroresonance suppression circuit in capacitor voltage transformers', *Int. J. Electr. Power Energy Syst.*, 2018, **99**, pp. 281–289, doi: 10.1016/j.ijepes.2018.01.021

[20] Yang, M., Sima, W., Chen, L., *et al.*: 'Suppressing ferroresonance in potential transformers using a model-free active resistance controller', *Int. J. Electr. Power Energy Syst.*, 2018, **95**, pp. 384–393, doi: 10.1016/j.ijepes.2017.08.035

[21] Diaz, F.J., Lopez, V.M., Azcondo, F.J., *et al.*: 'Contribution to digital power factor correction controllers in high intensity discharge lamps electronic ballast applications', *IET Power Electron.*, 2014, **7**, (7), pp. 1886–1894, ISSN 1755-4535, doi: 10.1049/iet-pel.2013.0401

[22] Azcondo, F.J., Diaz, F.J., Brañas, C., *et al.*: 'Microcontroller power mode stabilized power factor correction stage for high intensity discharge lamp electronic ballast', *IEEE Trans. Power Electron.*, 2007, **22**, (3), pp. 845–853, ISSN 0885-8993, doi: 10.1109/TPEL.2007.896509

[23] Azcondo, F.J., Branas, C., Casanueva, R., *et al.*: 'Power-mode-controlled power-factor corrector for electronic ballast', *IEEE Trans. Ind. Electron.*, 2005, **52**, (1), pp. 56–65, doi: 10.1109/tie.2004.841140

[24] Liu, J., Chan, K.W., Chung, C.Y., *et al.*: 'Single-stage wireless-power-transfer resonant converter with boost bridgeless power-factor-correction rectifier', *IEEE Trans. Ind. Electron.*, 2018, **65**, (3), pp. 2145–2155, ISSN 0278-0046, doi: 10.1109/TIE.2017.2745471

[25] Shen, X., Yan, T., Li, Q., *et al.*: 'Variable on-time controlled boundary conduction mode single-ended primary inductor converter power factor correction converter', *Electron. Lett.*, 2018, **54**, (2), pp. 97–99, ISSN 0013-5194, doi: 10.1049/el.2017.3837

[26] Qu, Z., Ebrahimi, S., Amiri, N., *et al.*: 'Adaptive method for stabilizing DC distribution systems with constant power loads based on active damping'. The 19th IEEE Workshop on Control and Modeling for Power Electronics, Padua, Italy, June 2018

[27] Bayona, E., Azcondo, F.J., Branas, C., *et al.*: 'Ferroresonance mitigation device in voltage transformers with a flyback based resistor emulator'. 19th IEEE Workshop on Control and Modeling for Power Electronics, Padua, Italy, June 2018

[28] Maksimovic, D., Jang, Y., Erickson, R.W.: 'Nonlinear-carrier control for high-power-factor boost rectifiers', *IEEE Trans. Power Electron.*, 1996, **11**, (4), pp. 578–584, ISSN 0885-8993, doi: 10.1109/63.506123

[29] Vamanan, N., John, V.: 'Dual comparison one cycle control for single phase AC to DC converters', *IEEE Trans. Ind. Appl.*, 2016, **52**, (4), pp. 3267–3278, ISSN 0093-9994, doi: 10.1109/TIA.2016.2555903

8 Appendix

8.1 Resistive emulator design

For design purposes of the circuit in Fig. 3, the evaluated power converter is modelled by the LFR concept. At the DC side

$$\frac{1}{R_{\mathrm{L}}}v_{\mathrm{o}}(t)+C_{\mathrm{o}}\frac{\mathrm{d}}{\mathrm{d}t}v_{\mathrm{o}}(t)=\frac{1}{R'_{\mathrm{d}}}\frac{v_{\Delta}^{2}(t)}{v_{\mathrm{o}}(t)}, \tag{22}$$

where the term $(1/R'_{\mathrm{d}})(v_{\Delta}^{2}(t)/v_{\mathrm{o}}(t))$ ensures that the power virtually dissipated at R'_{d} flows to the DC side of the power converter.

Solving the first-order differential equation in (22), the output voltage is given by

$$v_{\mathrm{o}}^{2}(t)=\frac{2}{C_{\mathrm{o}}}\mathrm{e}^{-(2t/C_{\mathrm{o}}R_{\mathrm{L}})}\int_{0}^{t}\frac{v_{\Delta}^{2}(\tau)}{R'_{\mathrm{d}}(\tau)}\mathrm{e}^{(2\tau/C_{o}R_{\mathrm{L}})}\,\mathrm{d}\tau, \tag{23}$$

where, due to the absence of a voltage control loop, the instantaneous output voltage values depend on the open-delta voltage, the emulated resistance and the selected C_{o} and R_{L}.

Assuming that the resistor emulator achieves the ferroresonance damping at the AC side, the resistor emulator behaviour can be approximated by

$$v_{\Delta}(t)\simeq\hat{V}_{\Delta}\,\mathrm{e}^{-(t/(T_{\mathrm{d}}/4))}\sin\frac{2\pi}{T_{\mathrm{FR}}}t \tag{24}$$

$$R'_{\mathrm{d}}\simeq R_{1}\left(1-\frac{R_{2}}{R_{1}}\mathrm{e}^{-(t/(T/4))}\right) \tag{25}$$

$$v_{\mathrm{o}}^2(t) = \frac{2\hat{V}_{\Delta}^2 \mathrm{e}^{-(2t/C_{\mathrm{o}}R_{\mathrm{L}})}}{R_1 C_{\mathrm{o}}} \int_0^t \frac{\sin^2 \omega_{\mathrm{r}}\tau}{\mathrm{e}^{-(2\tau/(C_{\mathrm{o}}R_{\mathrm{L}}T_{\mathrm{d}}))(T_{\mathrm{d}}-4C_{\mathrm{o}}R_{\mathrm{L}})} - (R_2/R_1)\,\mathrm{e}^{-(\tau/(T/4))-(2\tau/(C_{\mathrm{o}}R_{\mathrm{L}}T_{\mathrm{d}}))(T_{\mathrm{d}}-4C_{o}R_{\mathrm{L}})}} \mathrm{d}\tau\,. \tag{26}$$

$$v_{\mathrm{o}}(t) \simeq \hat{V}_{\Delta}\sqrt{\frac{1}{2}\frac{R_{\mathrm{L}}}{R_1 - R_2}}\sqrt{1 - \frac{\cos(22\pi/T_{\mathrm{FR}}t) + C_{\mathrm{o}}R_{\mathrm{L}}2\pi/T_{\mathrm{FR}}\sin(22\pi/T_{\mathrm{FR}}t)}{(C_{\mathrm{o}}R_{\mathrm{L}}2\pi/T_{\mathrm{FR}})^2 + 1}} \tag{28}$$

where it is considered that the main component in (1), at $2\pi/T_{\mathrm{FR}}\ rad/s$, is damped in T_{d} and the emulated resistance is modelled with (25). The behaviour of the applied emulated damping resistance, controlled with $g_{\mathrm{c}}(t)$, is characterised by means of R_1, R_2 and T. Time-invariant R'_{d} corresponds to $T \to \infty$ and time-variant R'_{d}, according to the proposed $g_{\mathrm{c}}(t) = G_{\mathrm{c}} + k_{\mathrm{G}}v_{\Delta}(t)$, is modelled by adjusting R_1, R_2 and T.

By substituting (24) and (25) into (23), the output voltage results in (see (26)) . Since T_{d} depend on the applied emulated resistance R'_{d} and the MV grid characteristics (e.g. line-to-ground parasitic capacitance, VT characteristics etc.) and, moreover, the values of T must be in the range of T_{d} (i.e. seconds), then, conditions $C_{\mathrm{o}}R_{\mathrm{L}} \ll (T_{\mathrm{d}}/4)$ and $C_{\mathrm{o}}R_{\mathrm{L}} \ll (T/2)$ can be imposed by design and, then, (26) is approached by

$$v_{\mathrm{o}}^2(t) \simeq \frac{2\hat{V}_{\Delta}^2}{(R_1 - R_2)C_{\mathrm{o}}}\mathrm{e}^{-(2t/C_{\mathrm{o}}R_{\mathrm{L}})}\int_0^t \mathrm{e}^{(2\tau/C_{\mathrm{o}}R_{\mathrm{L}})}\sin^2\frac{2\pi}{T_{\mathrm{FR}}}\tau\,\mathrm{d}\tau \tag{27}$$

which results in (see (28)) where the average output voltage is adjusted by means of the selected R_1, R_2 and R_{L} values and depends on the initial amplitude of the open-delta voltage $\hat{V}_{\Delta}$ while the output voltage ripple depends on R_{L}, C_{o} and $2\pi/T_{\mathrm{FR}}$.

Once the DSO establishes the worst-case value of $\hat{V}_{\Delta}$, due to the MV grid characteristics, and the required values of R_1 and R_2, preventing VT damage and ensuring system stability, the R_{L} and C_{o} values are selected to obtain a low enough value of the output voltage (preventing the output capacitor damaging) and minimising the output voltage ripple. Using R_1 and R_2, and considering the employed topology, the values of G_{c} and k_{G} are adjusted.